ACTIVE BUCKLING CONTROL OF AN AXIALLY LOADED BEAM-COLUMN WITH CIRCULAR CROSS-SECTION BY ACTIVE SUPPORTS WITH INTEGRATED PIEZOELECTRIC ACTUATORS

Maximilian Schaeffner[*]**, Roland Platz**[†]**, Tobias Melz**[*]

[*]System Reliability and Machine Acoustics SzM, Technische Universität Darmstadt
Magdalenenstraße 4, D-64289 Darmstadt, Germany
schaeffner@szm.tu-darmstadt.de, melz@szm.tu-darmstadt.de

[†]Fraunhofer Institute for Structural Durability and System Reliability LBF
Bartningstraße 47, D-64289 Darmstadt, Germany
roland.platz@lbf.fraunhofer.de

Keywords: smart structures, modeling, active buckling control, active supports, beam-column stabilization.

Summary: *Buckling of slender beam-columns subject to axial compressive loads represents a critical design constraint for light-weight structures. Passive solutions to increase the critical buckling load are limited by increasing or modifying the cross-sectional area, changing the material or reducing the beam-column length and may lead to oversizing or unwanted change in geometry. Active buckling control provides a possible alternative to stabilize slender beam-columns by active lateral forces or bending moments with fewer modifications in geometry, shape and material. In this paper, the potential of active buckling control of an axially loaded beam-column with circular solid cross-section by active supports with integrated piezoelectric actuators at both ends is investigated numerically. The beam-column itself stays free from any geometrical or material modifications along its length. A mathematical model of the axially loaded beam-column is derived and a linear quadratic regulator (LQR) with state observer is designed to stabilize the system. The effectiveness of the stabilization concept is investigated by numerical simulation of the supercritically loaded beam-column. With the proposed active buckling control it is possible to increase the maximum bearable axial compressive load significantly above the first critical buckling load of the passive beam-column.*

1. INTRODUCTION

Buckling of slender and compressively loaded beam-columns is a critical failure mode in the design of light-weight structures. The theory of buckling for passive beam-columns has been thoroughly investigated, [1]. A general approach to passively increase the critical buckling load is to change the geometry, e. g. length and cross-section area, or the material so that it withstands higher loads. This, however, is sometimes not desirable because of given design constraints.

Maximilian Schaeffner, Roland Platz, Tobias Melz

In these cases, active buckling control without significant change in geometry and material provides a suitable approach to increase the maximum bearable load of a given structure.

Active buckling control of slender beam-columns with rectangular cross-section and different boundary conditions has been investigated numerically and experimentally several times and an increase in the critical buckling load could be achieved in all cases, [2, 3, 4, 5, 6, 7, 8, 9]. One way to compare the different investigated structures is to compare the slenderness ratio $s = l_{\text{eff}}/i$ that is derived from the beam's effective buckling length l_{eff} and the gyration radius i. Usually, elastic EULER buckling may occur for slenderness ratios higher than the limiting slenderness ratio $s > s_{\text{l}} = \pi \sqrt{E/\sigma_{\text{p}}}$ which is dependent on the material's Young's modulus E and the proportional limit σ_{p}. The higher s, the more vulnerable a beam-column is against buckling.

Often, surface bonded piezoelectric patches were used to induce active bending moments in the structure to counteract the deformation, [2, 3, 4, 5]. In a numerical study, the buckling load of a pinned-pinned beam with piezoelectric patches along the entire length and slenderness ratio $s = 530$ could be increased above the first critical buckling load by $280\,\%$ for slow static load variations, [2]. In a similar numerical study with the same beam geometry with pinned-pinned boundary conditions and discrete piezo patches at two beam positions, an increase in the critical buckling load by $780\,\%$ was achieved for the stabilization of a non-zero initial deflection, [3]. The experimental studies generally achieved a smaller increase in critical buckling load than the numerical studies. In [4], actively controlled piezoelectric patches were applied to predeflected carbon-epoxy composite columns with slenderness ratio $s = 970$ and the critical buckling load could be increased by $37\,\%$ compared to the column without actively controlled patches and by $7\,\%$ compared to the theoretical buckling load of the undeflected column. For a beam-column with $s = 670$ and active piezoelectric patch actuators attached along the entire surface with additional stiffeners to cover gaps between the actuators, the buckling load of the passive system could be increased by $460\,\%$, [5]. In another stabilization concept, a predeflected beam-column with $s = 300$ and eccentrically embedded shape memory alloys was investigated experimentally and an increase of $11\,\%$ in the critical buckling load was achieved, [6].

The active stabilization concept investigated by earlier own studies used piezoelectric stack actuators to apply active lateral forces near the base of a fixed-pinned beam-column with rectangular cross-section and slenderness ratio $s = 725$, [7, 8, 9]. Compared to other studies mentioned above, most of the beam-column's surface was kept free from any actuator like piezoelectric patches, so the beam-column's stiffness and, respectively, the slenderness ratio was not influenced by additional actuators. Only strain gauges were applied on the surface. In the earlier own studies, a lateral disturbance force represented uncertainty in loading of the beam-column that had to be compensated by the buckling control. In an experimental study, an increase in the critical axial buckling load of $40\,\%$ was achieved by using a linear-quadratic regulator (LQR) to control the first three modes of the supercritically loaded beam-column, [9].

Active buckling control of beam-columns with circular cross-section has not often been investigated so far. In [10], active buckling control of a circular beam-column with slenderness ratio $s = 500$ and active lateral forces acting near the beam-column's fixed base was investigated. An increase of $110\,\%$ in the critical buckling load was achieved in a numerical simulation.

The studies mentioned before investigated beam-columns with high slenderness ratios $s \geq 300$ with low stiffness and relatively low buckling loads. In this paper, a rather stiff beam-column is stabilized using active supports with integrated piezoelectric actuators to introduce active lateral forces below the beam-column ends. The beam-column has a first critical buckling load of $P_{\mathrm{cr},1} = 3221.3\,\mathrm{N}$ and a relatively low slenderness ratio $s = 104$ that is closer to the limiting slenderness ratio of $s_{\mathrm{l}} = 38$ of the chosen material than in earlier studies.

2. SYSTEM DESCRIPTION AND STABILIZATION CONCEPT

The investigated system is a slender beam-column of length l_{b} with circular solid cross-section of radius r_{b} that has two elastic supports A at $x = 0$ and B at $x = l_{\mathrm{b}}$ with rotational stiffness k_{φ} and lateral stiffness k_{l} that are the same for both supports A and B and in both y- and z- direction, Fig. 1. The beam-column properties radius r_{b}, bending stiffness EI_{b} and density ρ_{b} are assumed to be constant across the entire beam-column length l_{b}.
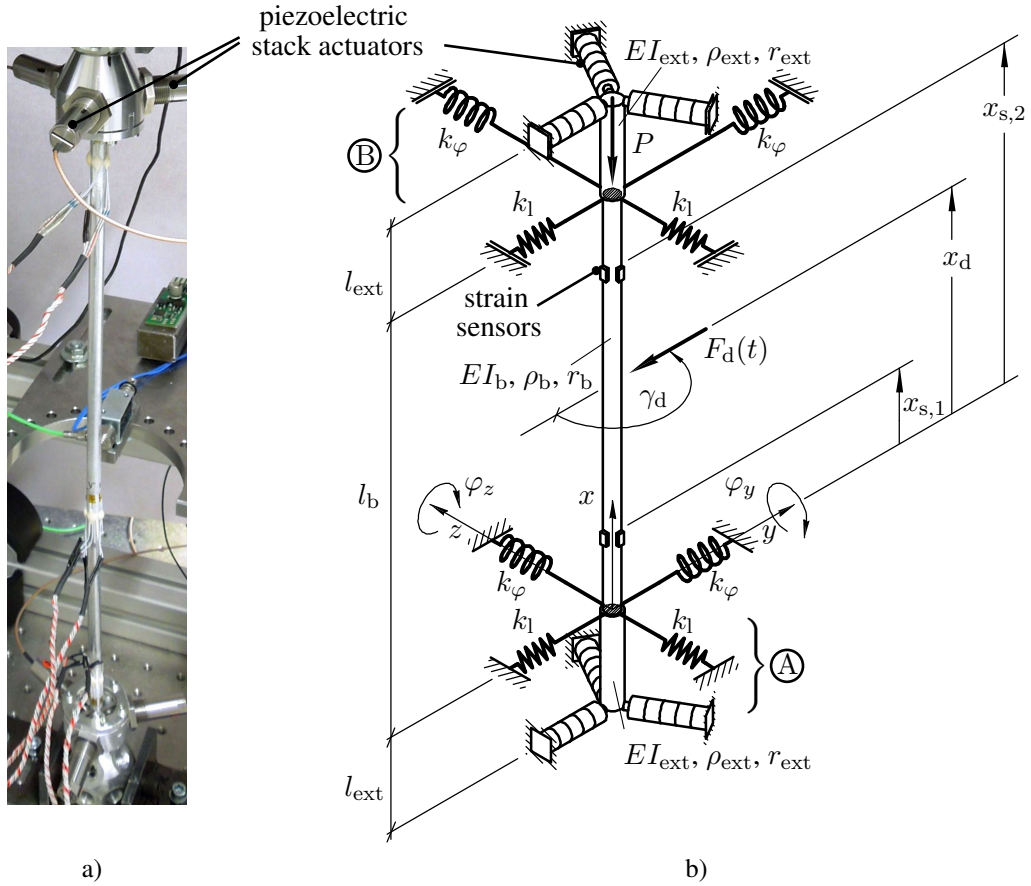

Figure 1: Beam-column system, a) beam-column with active supports for experimental test, b) sketch of beam-column

3

Maximilian Schaeffner, Roland Platz, Tobias Melz

In each support A and B at position $x = -l_\mathrm{ext}$ and $x = l_\mathrm{b} + l_\mathrm{ext}$, three piezoelectric stack actuators are arranged in the support housing at an angle of $120\,^\circ$ to each other in one plane orthogonal to the beam-column's x-axis. They are connected to the beam-column via a relatively stiff axial extension of length l_ext, radius r_ext, bending stiffness EI_ext and density ρ_ext forming a cantilever beam ending beyond both spring elements. This way, active lateral forces in arbitrary directions orthogonal to the beam-column's longitudinal x-axis can be introduced in both supports A and B, Sec. 3. The beam-column is loaded with a constant axial load P that exceeds the first critical axial buckling load $P > P_\mathrm{cr,1}$. The circular cross-section has no preferred direction of buckling, so the beam-column may buckle in any plane lateral to the x-axis. A time-dependent lateral impulse disturbance force $F_\mathrm{d}(t)$ that initially deflects the beam-column is applied at x_d with variable angle $90\,^\circ \leq \gamma_\mathrm{d} \leq 270\,^\circ$. Two sensors at position $x_\mathrm{s,1/2}$ are used to identify the lateral displacement of the beam-column in y- and z-direction.

Figure 2 shows the close-up view of the beam-column support A in the experimental test setup and a sectional view of the CAD-model. The support housing and beam-column material is aluminum alloy EN AW-7075-T6 and the axial extension material is hardened steel 1.2312. The elastic spring element that bears the axial compressive load and allows rotations in any plane perpendicular to the x-axis is made of spring steel 1.4310.
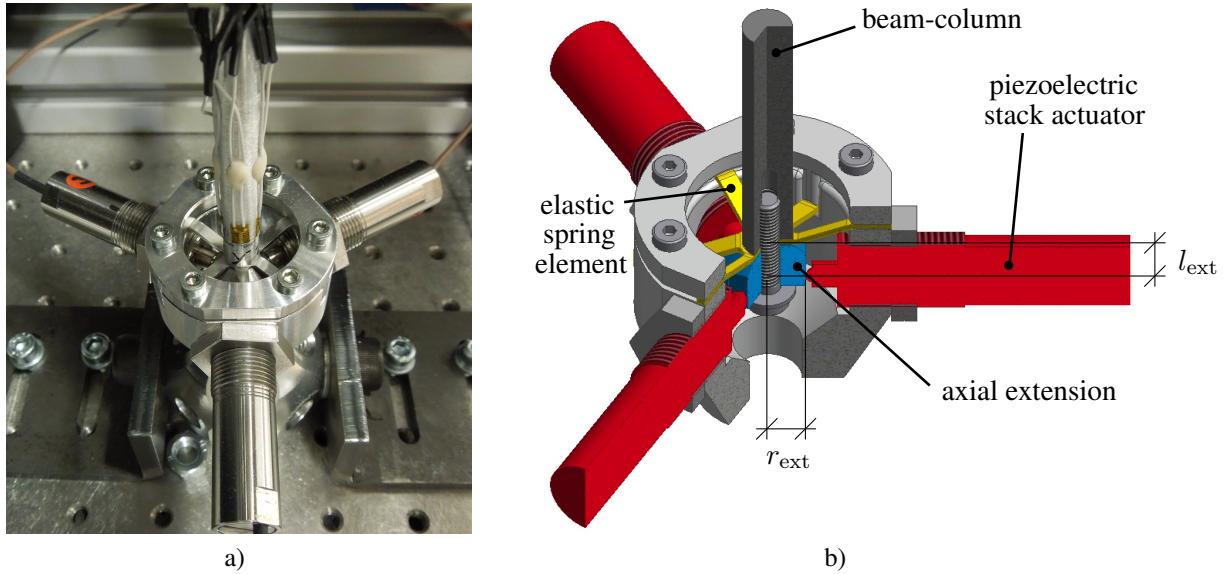

Figure 2: Active support A, a) active support in experimental test setup, b) sectional view of active support in CAD-model with elastic spring element and piezoelectric stack actuators acting on an axial extension of radius r_ext of the beam-column at a distance of l_ext

The model parameters describing the properties of the beam-column system presented in Figures 1 and 2 are summarized in Table 1.

property	symbol	value	SI-unit
beam-column length	l_b	0.4	m
beam-column radius	r_b	0.004	m
axial extension length	l_ext	0.0075	m
axial extension radius	l_ext	0.006	m
sensor positions	$[x_\mathrm{s,1},\ x_\mathrm{s,2}]$	$[0.03,\ 0.37]$	m
Young's modulus aluminum EN AW-7075-T6	E_b	$70.0 \cdot 10^9$	N/m^2
density aluminum EN AW-7075-T6	ρ_b	2710	kg/m^3
proportional limit aluminum EN AW-7075-T6	$\sigma_\mathrm{p,b}$	$485.0 \cdot 10^6$	N/m^2
Young's modulus steel 1.2312	E_ext	$210.0 \cdot 10^9$	N/m^2
density steel 1.2312	ρ_ext	7810	kg/m^3
rotational stiffness spring element	k_φ	415.3	Nm/rad
lateral stiffness spring element	k_l	$60.81 \cdot 10^6$	N/m
lateral stiffness piezoelectric stack actuator	k_p	$22 \cdot 10^6$	N/m

Table 1: Properties of the active beam-column system

3. MATHEMATICAL MODEL AND CONTROLLER DESIGN

For the active buckling control of the supercritically loaded beam-column, a mathematical model of the beam-column for controller design is needed. In a first step, a finite element (FE) model of the beam-column is developed, Sec. 3.1. In a second step, a reduced state space model is set up, Sec. 3.2, which is then used to design a stabilizing controller and observer, Sec. 3.3.

3.1 Finite Element Model

To describe the lateral motion of the beam-column with constant axial load P, a FE-model of the beam-column system, Fig. 1b, is used. The beam-column and the stiff extensions are discretized by $N - 1$ one-dimensional BERNOULLI beam elements of length l_el with N nodes that each have four degrees of freedom, Fig. 3a. Each node n is described by the lateral displacements v_n and w_n in y- and z-direction and the rotational displacements $\varphi_{y,n}$ and $\varphi_{z,n}$ around the y- and z-axis. Consequently, the $[4N \times 1]$ FE-displacement vector is

$$\mathbf{v}(t) = [v_1(t),\ w_1(t),\ \varphi_{y,1}(t),\ \varphi_{z,}(t), \dots, v_N(t),\ w_N(t),\ \varphi_{y,N}(t),\ \varphi_{z,N}(t)]^T . \tag{1}$$

Axial and rotational displacements in and around the x-axis of the beam-column are neglected.
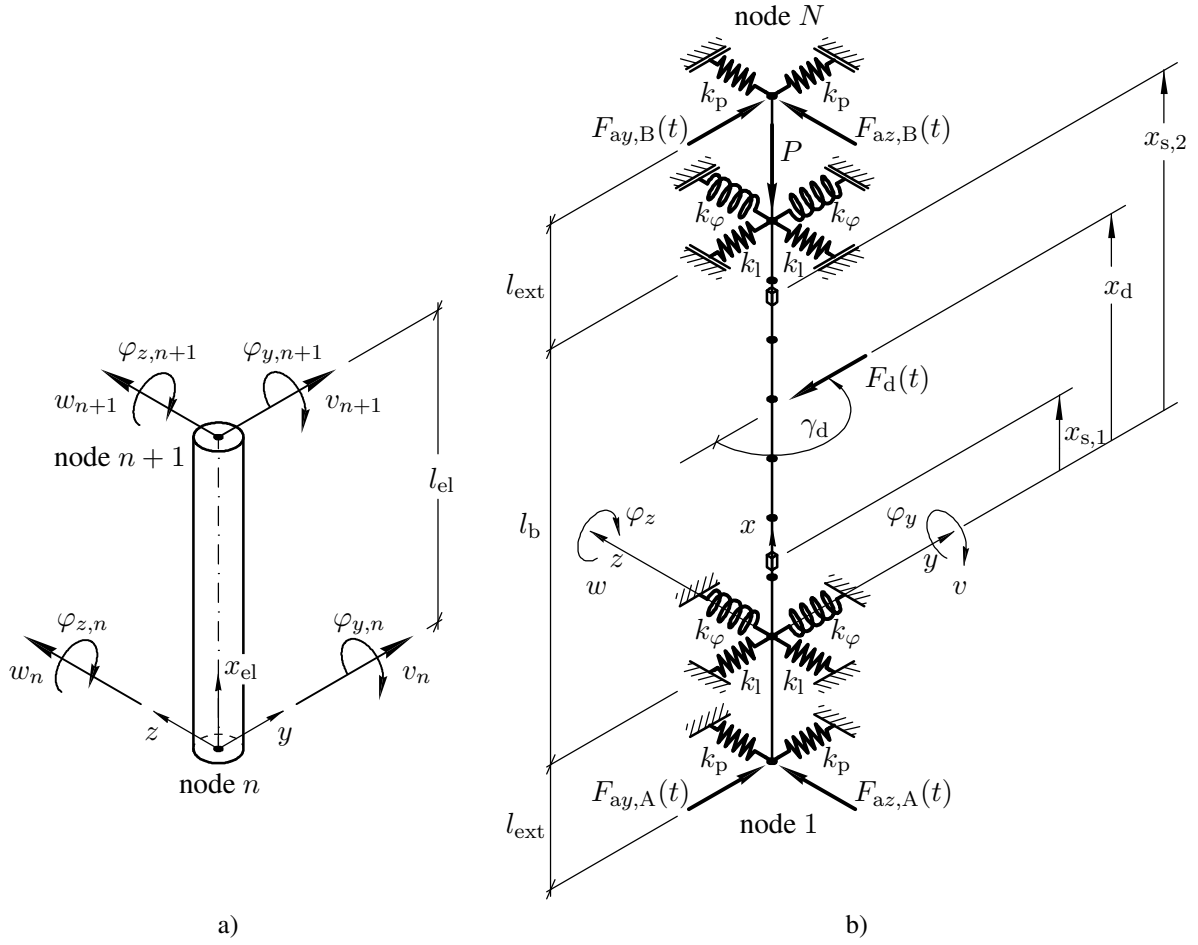
Figure 3: FE-beam-column system, a) nth finite beam-column element $1 \leq n \leq N-1$ of length l_{el} with element coordinates in positive directions, b) FE-model of beam-column

Figure 3b shows the discretized beam-column with $N-1$ finite elements and N nodes. The beam-column is loaded by the constant axial load P acting at node $N-1$ and disturbed by the lateral force $F_{\mathrm{d}}(t)$ acting at x_{d} with angle $90\,^\circ \leq \gamma_{\mathrm{d}} \leq 270\,^\circ$. The piezoelectric stack actuators in the beam-column supports A and B are represented by the lateral stiffness k_{p} and additional active control forces $F_{\mathrm{a}y/z,\mathrm{A}/\mathrm{B}}(t)$ in the y- and z-direction of nodes 1 and N of the FE-model. The active forces are summarized in the control input vector

$$\mathbf{u}(t) = \begin{bmatrix} F_{\mathrm{a}y,\mathrm{A}}(t) \\ F_{\mathrm{a}y,\mathrm{B}}(t) \\ F_{\mathrm{a}z,\mathrm{A}}(t) \\ F_{\mathrm{a}z,\mathrm{B}}(t) \end{bmatrix}. \tag{2}$$

The GALERKIN method with cubic HERMITIAN shape functions $\mathbf{g}(x_{\mathrm{el}})$ is used to build the $[8 \times 8]$ element stiffness matrix $\mathbf{K}_{\mathrm{el}}(P)$ and element mass matrix $\mathbf{M}_{\mathrm{el}}$ for the BERNOULLI beam

6

elements, [11]. The element stiffness matrix takes into account the influence of the axial force via

$$\mathbf{K}_{\mathrm{el}}(P) = \mathbf{K}_{\mathrm{e,el}} - P\,\mathbf{K}_{\mathrm{g,el}} \tag{3}$$

with elastic element stiffness matrix $\mathbf{K}_{\mathrm{e,el}}$ and geometric element stiffness matrix

$$\mathbf{K}_{\mathrm{g,el}} = \frac{1}{l_{\mathrm{el}}}\begin{pmatrix} 6/5 & 0 & 0 & l_{\mathrm{el}}/10 & -6/5 & 0 & 0 & l_{\mathrm{el}}/10 \\ & 6/5 & -l_{\mathrm{el}}/10 & 0 & 0 & -6/5 & -l_{\mathrm{el}}/10 & 0 \\ & & 2/15\,l_{\mathrm{el}}^2 & 0 & 0 & l_{\mathrm{el}}/10 & -l_{\mathrm{el}}^2/30 & 0 \\ & & & 2/15\,l_{\mathrm{el}}^2 & -l_{\mathrm{el}}/10 & 0 & 0 & -l_{\mathrm{el}}^2/30 \\ & & & & 6/5 & 0 & 0 & -l_{\mathrm{el}}/10 \\ & & & & & 6/5 & l_{\mathrm{el}}/10 & 0 \\ & & \text{symmetric} & & & & 2/15\,l_{\mathrm{el}}^2 & 0 \\ & & & & & & & 2/15\,l_{\mathrm{el}}^2 \end{pmatrix} \tag{4}$$

that describes the influence of the axial load P on the beam-column's lateral stiffness. The elastic element stiffness matrix $\mathbf{K}_{\mathrm{e,el}}$ and element mass matrix $\mathbf{M}_{\mathrm{el}}$ are readily found in literature, [11, 12]. After assembling the global stiffness and mass matrices from the element matrices, the FE-equation of motion is

$$\mathbf{M}\,\ddot{\mathbf{v}}(t) + \mathbf{D}(P)\,\dot{\mathbf{v}}(t) + \mathbf{K}(P)\,\mathbf{v}(t) = \mathbf{B}_0\,\mathbf{u}(t) + \mathbf{b}_{\mathrm{d}}\,F_{\mathrm{d}}(t). \tag{5}$$

In Eq. (5), the $[4N \times 4N]$ global stiffness matrix $\mathbf{K}(P) = \mathbf{K}_{\mathrm{e}} - P\,\mathbf{K}_{\mathrm{g}}$ consists of the stiffness element matrices, Eq. (3), as a function of the constant axial load P with the global elastic stiffness matrix $\mathbf{K}_{\mathrm{e}}$ and the global geometric stiffness matrix $\mathbf{K}_{\mathrm{g}}$, Eq. (4). The lateral stiffness k_{p} of the piezoelectric stack actuators is added to the entries of the lateral degrees of freedom of nodes 1 and N in the global elastic stiffness matrix $\mathbf{K}_{\mathrm{e}}$. Similarly, the lateral and rotational stiffness k_{l} and k_{φ} of the global elastic spring elements are added to the entries of the lateral and rotational degrees of freedom of nodes 2 and $N-1$ in the elastic stiffness matrix $\mathbf{K}_{\mathrm{e}}$. The first and second critical buckling loads $P_{\mathrm{cr,1}}$ and $P_{\mathrm{cr,2}}$ of the beam-column with the given boundary conditions are calculated according to [12] from the global elastic and geometric stiffness matrices by solution of the eigenvalue problem

$$\det\left[\mathbf{K}_{\mathrm{e}} - P_{\mathrm{cr,1/2}}\,\mathbf{K}_{\mathrm{g}}\right] = 0. \tag{6}$$

The further terms in Eq. (5) are the global mass matrix $\mathbf{M}$ and the global damping matrix $\mathbf{D}(P)$ that is determined by RAYLEIGH proportional damping $\mathbf{D}(P) = \alpha\,\mathbf{M} + \beta\,\mathbf{K}(P)$, [13]. The proportional damping coefficients α and β are determined for assumed modal damping ratios of the first two bending modes of $\zeta_{1/2} = 1\,\%$. The right hand side of Eq. (5) represents the external forces that are the active control forces $\mathbf{u}(t)$, Eq. (2), and the lateral disturbance force $F_{\mathrm{d}}(t)$. The $[4N \times 4]$ control input matrix $\mathbf{B}_0$ maps the active forces of the control input vector $\mathbf{u}(t)$ to the lateral degrees of freedom of the first and last nodes 1 and N of the FE-model. Similarly, the disturbance force $F_{\mathrm{d}}(t)$ is mapped to the FE-nodes according to the disturbance position x_{d} and the disturbance angle γ_{d} via $[4N \times 1]$ disturbance input vector $\mathbf{b}_{\mathrm{d}}$.

The lateral motion $v(t)$ and $w(t)$ of the beam-column in the real test setup is measured with eight strain gauge sensors that are applied on the beam-column surface at two sensor positions $x_{\mathrm{s},1/2}$ in the y- and z-direction, Fig. 1. Therefore, the surface strain at the sensor positions in the y- and z-direction is chosen as output

$$\mathbf{y}(t) = \begin{bmatrix} \varepsilon_y(x_{\mathrm{s},1}, t) \\ \varepsilon_z(x_{\mathrm{s},1}, t) \\ \varepsilon_y(x_{\mathrm{s},2}, t) \\ \varepsilon_z(x_{\mathrm{s},2}, t) \end{bmatrix} = \mathbf{C}_0\,\mathbf{v}(t). \tag{7}$$

In Eq. (7), the $[4 \times 4N]$ output matrix $\mathbf{C}_0$ relate the surface strains $\mathbf{y}(t)$ to the FE-displacement vector $\mathbf{v}(t)$, Eq. (1), by the entries $-r_{\mathrm{b}}\,\mathbf{g}''(x_{\mathrm{s},1/2})$ at the FE-nodes surrounding sensor positions $x_{\mathrm{s},1/2}$ where r_{b} is the beam-column radius and $\mathbf{g}''(x_{\mathrm{el}})$ the second derivative of the HERMITIAN shape functions, [11].

3.2 Reduced State Space Model

For the full state FE-model, Eq. (5), a relatively high number of $N = 53$ nodes resulting in $4N = 212$ degrees of freedom is chosen to properly describe the maximum surface strain at the sensor positions $x_{\mathrm{s},1/2}$ according to Eq. (7). Once the maximum surface strain is known, the FE-model is reduced for further simulation and controller design. First, a modal reduction of the FE-model is performed so that higher modes are excluded from the calculation of the beam-column's dynamic behavior. Secondly, a model reduction via balanced truncation is carried out so that the model is optimized for the controller design, Sec. 3.3.

A modal reduction of the FE-model that only includes a limited number of $p < 4N$ of the system's mode shapes is conducted in this work. The vector of modal displacements $\mathbf{q}_{\mathrm{M}}(t)$ is calculated from the full state FE-displacement vector via the transformation

$$\mathbf{v}(t) = \mathbf{\Phi}\,\mathbf{q}_{\mathrm{M}}(t), \tag{8}$$

with the $[4N \times p]$ modal matrix

$$\mathbf{\Phi} = [\mathbf{\Phi}_1, \mathbf{\Phi}_2, \dots \mathbf{\Phi}_p] \tag{9}$$

including the first p eigenvectors of the FE-Model, [14].

The eigenvectors in Eq. (9) are normalized with respect to the mass matrix $\mathbf{M}$, so that the modal mass matrix $\widetilde{\mathbf{M}}$, modal stiffness matrix $\widetilde{\mathbf{K}}$ and modal damping matrix $\widetilde{\mathbf{D}}$ result in the diagonal matrices

$$\widetilde{\mathbf{M}} = \mathbf{\Phi}^T\,\mathbf{M}\,\mathbf{\Phi} = \mathbf{I}^{[p \times p]}$$
$$\widetilde{\mathbf{K}}(P) = \mathbf{\Phi}^T\,\mathbf{K}\,\mathbf{\Phi} = \mathrm{diag}\left[\omega_1^2(P), \dots, \omega_p^2(P)\right] \tag{10}$$
$$\widetilde{\mathbf{D}}(P) = \mathbf{\Phi}^T\,\mathbf{D}\,\mathbf{\Phi} = \mathrm{diag}\left[2\,\zeta_1(P)\,\omega_1(P), \dots, 2\,\zeta_p(P)\,\omega_p(P)\right]$$

with identity matrix $\mathbf{I}$, the eigen angular frequencies $\omega_i(P)$ and the modal damping ratios $\zeta_i(P)$ as functions of the axial load P and $i = 1 \dots p$.

Using the $[2p \times 1]$ modal state vector $\mathbf{x}_\mathrm{M}(t) = [\mathbf{q}_\mathrm{M}(t), \dot{\mathbf{q}}_\mathrm{M}(t)]^T$ with the modal displacements and velocities, the modal state space equations of first order are

$$\dot{\mathbf{x}}_\mathrm{M}(t) = \begin{bmatrix} 0 & \mathbf{I}^{[p \times p]} \\ -\widetilde{\mathbf{K}}(P) & -\widetilde{\mathbf{D}}(P) \end{bmatrix} \mathbf{x}_\mathrm{M}(t) + \begin{bmatrix} 0 \\ \mathbf{\Phi}^T \mathbf{B}_0 \end{bmatrix} \mathbf{u}(t) + \begin{bmatrix} 0 \\ \mathbf{\Phi}^T \mathbf{b}_\mathrm{d} \end{bmatrix} F_\mathrm{d}(t)$$

$$\mathbf{y}(t) = \begin{bmatrix} \mathbf{C}_0 \, \mathbf{\Phi} & 0 \end{bmatrix} \mathbf{x}_\mathrm{M}(t),$$

(11)

[14], leading to the reduced modal state space form of Eq. (5)

$$\dot{\mathbf{x}}_\mathrm{M}(t) = \mathbf{A}_\mathrm{M}(P) \, \mathbf{x}_\mathrm{M}(t) + \mathbf{B}_\mathrm{M} \, \mathbf{u}(t) + \mathbf{b}_\mathrm{dM} \, F_\mathrm{d}(t)$$

$$\mathbf{y}(t) = \mathbf{C}_\mathrm{M} \, \mathbf{x}_\mathrm{M}(t).$$

(12)

Finally, a balanced realization of the beam-column's modal state space model, Eq. (12), is set up with the transformation

$$\mathbf{x}_\mathrm{b}(t) = \mathbf{T}_\mathrm{b} \, \mathbf{x}_\mathrm{M}(t)$$

(13)

using MATLAB *balreal* function. The resulting state space system with balanced system matrix $\mathbf{A}_\mathrm{b}(P)$, balanced control input matrix $\mathbf{B}_\mathrm{b}$, balanced disturbance input vector $\mathbf{b}_\mathrm{d,b}$ and balanced output matrix $\mathbf{C}_\mathrm{b}$ is ordered according to the highest HANKEL singular values that express the energy of the system states $\mathbf{x}_\mathrm{M}(t)$, [15]. The balanced state vector and matrices are then divided into a reduced balanced system with a reduced number of $r < 2p$ states, index r, and an eliminated balanced system with $2p - r$ states, index e, according to

$$\mathbf{x}_\mathrm{b}(t) = \begin{bmatrix} \mathbf{x}_\mathrm{b,r}(t) \\ \mathbf{x}_\mathrm{b,e}(t) \end{bmatrix}$$

$$\mathbf{A}_\mathrm{b}(P) = \mathbf{T}_\mathrm{b}^{-1} \, \mathbf{A}_\mathrm{M}(P) \, \mathbf{T}_\mathrm{b} = \begin{bmatrix} \mathbf{A}_\mathrm{b,r}(P) & \mathbf{A}_\mathrm{b,1}(P) \\ \mathbf{A}_\mathrm{b,2}(P) & \mathbf{A}_\mathrm{b,e}(P) \end{bmatrix}$$

$$\mathbf{B}_\mathrm{b}(P) = \mathbf{T}_\mathrm{b} \, \mathbf{B}_\mathrm{M} = \begin{bmatrix} \mathbf{B}_\mathrm{b,r} \\ \mathbf{B}_\mathrm{b,e} \end{bmatrix}$$

(14)

$$\mathbf{b}_\mathrm{d,b}(P) = \mathbf{T}_\mathrm{b} \, \mathbf{b}_\mathrm{d,M} = \begin{bmatrix} \mathbf{b}_\mathrm{d,b,r} \\ \mathbf{b}_\mathrm{d,b,e} \end{bmatrix}$$

$$\mathbf{C}_\mathrm{b}(P) = \mathbf{C}_\mathrm{M} \, \mathbf{T}_\mathrm{b}^{-1} = \begin{bmatrix} \mathbf{C}_\mathrm{b,r} & \mathbf{C}_\mathrm{b,e} \end{bmatrix}.$$

The second part $\mathbf{x}_\mathrm{b,e}(t)$ of the balanced state vector $\mathbf{x}_\mathrm{b}(t)$ contains all poorly observable and controllable states so that these are eliminated (truncated) from the model, [15]. The resulting state space system for the $[r \times 1]$ reduced state vector $\mathbf{x}_\mathrm{b,r}(t)$ can be written as

$$\dot{\mathbf{x}}_\mathrm{r}(t) = \mathbf{A}_\mathrm{b,r}(P) \, \mathbf{x}_\mathrm{b,r}(t) + \mathbf{B}_\mathrm{b,r} \, \mathbf{u}(t) + \mathbf{b}_\mathrm{d,b,r} \, F_\mathrm{d}(t) \tag{15}$$

$$\mathbf{y}(t) = \mathbf{C}_\mathrm{b,r} \, \mathbf{x}_\mathrm{b,r}(t). \tag{16}$$

For simplicity, the reduced matrices in the following are written as $\mathbf{A} = \mathbf{A}_\mathrm{b,r}(P)$, $\mathbf{B} = \mathbf{B}_\mathrm{b,r}$ and $\mathbf{C} = \mathbf{C}_\mathrm{b,r}$ and the reduced system state vector as $\mathbf{x}(t) = \mathbf{x}_\mathrm{b,r}(t)$.

3.3 Controller and Observer Design

The instable reduced state space model of the supercritically loaded beam-column, Eqs. (15) and (16), is fully controllable and observable so that it is possible to design a stabilizing controller. The stabilization control of the circular beam-column is achieved by an infinite horizon, continuous-time linear quadratic regulator (LQR). The control law determines the control input $\mathbf{u}(t)$ from the system state vector $\mathbf{x}(t)$ so that the quadratic performance index

$$J = \int_0^\infty \left\{ \mathbf{x}^T(t)\, \mathbf{Q}\, \mathbf{x}(t) + \mathbf{u}^T(t)\, \mathbf{R}\, \mathbf{u}(t) \right\} \mathrm{d}t \tag{17}$$

is minimized, [16]. The matrices $\mathbf{Q}$ and $\mathbf{R}$ represent weights on the system state vector $\mathbf{x}(t)$ and the control input $\mathbf{u}(t)$, respectively. They are chosen as

$$\mathbf{Q} = \alpha\, \mathbf{C}^T\mathbf{C} \qquad \text{and} \qquad \mathbf{R} = \mathbf{I}^{[4\times4]} \tag{18}$$

with $\mathbf{C}$ from Eq. (16) so that the control parameter α is used to adjust the ratio between the weight matrices, [8, 9, 16]. The numerical simulations in this paper are performed with $\alpha = 1 \cdot 10^8$. The control input $\mathbf{u}(t)$, Eq. (2), is calculated by

$$\mathbf{u}(t) = -\mathbf{K}_{\mathrm{LQR}}\, \mathbf{x}(t), \tag{19}$$

where the control matrix $\mathbf{K}_{\mathrm{LQR}}$ is given by

$$\mathbf{K}_{\mathrm{LQR}} = \mathbf{R}^{-1}\, \mathbf{B}^T\, \mathbf{P}. \tag{20}$$

In Eq. (20), $[r \times r]$ matrix $\mathbf{P}$ is the solution of the continuous-time Algebraic RICCATI Equation (CARE)

$$\mathbf{A}^T\, \mathbf{P} + \mathbf{P}\, \mathbf{A} - \mathbf{P}\, \mathbf{B}\, \mathbf{R}^{-1}\, \mathbf{B}^T\, \mathbf{P} + \mathbf{Q} = 0 \tag{21}$$

with system matrix $\mathbf{A}$, input matrix $\mathbf{B}$, Eq. (15), and the LQR weights $\mathbf{Q}$ and $\mathbf{R}$, Eq. (18).

Since the system state vector $\mathbf{x}(t)$ is not directly measurable and only the beam-column strain $\mathbf{y}(t)$ is a measurable output, an observer is required to estimate the state vector $\mathbf{x}(t)$. The observer state space equation describing the estimated state vector $\widehat{\mathbf{x}}(t)$ is given by

$$\dot{\widehat{\mathbf{x}}}(t) = \mathbf{A}\, \widehat{\mathbf{x}}(t) + \mathbf{B}\, \mathbf{u}(t) + \mathbf{L}\, (\mathbf{y}(t) - \widehat{\mathbf{y}}(t)) \tag{22}$$
$$\widehat{\mathbf{y}}(t) = \mathbf{C}\, \widehat{\mathbf{x}}(t), \tag{23}$$

with the estimated output $\widehat{\mathbf{y}}(t)$ and the observer matrix $\mathbf{L}$, [17]. The setup of the used LUEN-BERGER observer for the beam-column system as control plant is shown in Fig. 4, [17, 18].
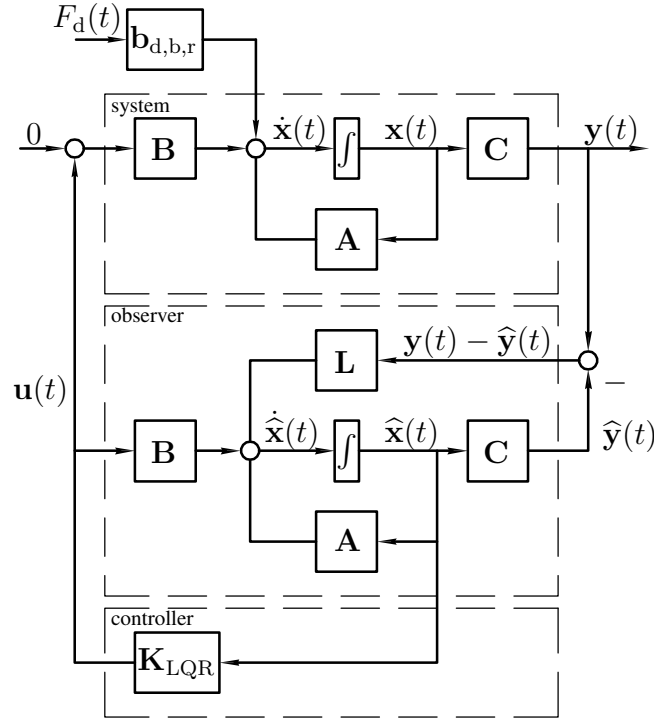
Figure 4: Closed loop control with LUENBERGER observer for state estimation

Using the estimated state vector to determine the control input $\mathbf{u}(t) = -\mathbf{K}_{\mathrm{LQR}}\,\widehat{\mathbf{x}}(t)$ and inserting Eq. (16) and Eq. (23) into Eq. (22) yields the state space equations for the state estimate error $\mathbf{e}(t) = \mathbf{x}(t) - \widehat{\mathbf{x}}(t)$ and the state vector $\mathbf{x}(t)$

$$
\begin{bmatrix} \dot{\mathbf{x}}(t) \\ \dot{\mathbf{e}}(t) \end{bmatrix} = \begin{bmatrix} \mathbf{A} - \mathbf{B}\,\mathbf{K}_{\mathrm{LQR}} & \mathbf{B}\,\mathbf{K}_{\mathrm{LQR}} \\ 0 & \mathbf{A} - \mathbf{L}\,\mathbf{C} \end{bmatrix} \begin{bmatrix} \mathbf{x}(t) \\ \mathbf{e}(t) \end{bmatrix}, \tag{24}
$$

[17].From Eq. (24) it can be seen that the controller and observer design results in two separate problems (separation principle), [18]. The closed loop eigenvalues of the controller $\mathbf{A} - \mathbf{B}\,\mathbf{K}_{\mathrm{LQR}}$ are determined by the LQR control, Eq. (20), to be stable and on the negative half-plane. The eigenvalues of the observer $\mathbf{A} - \mathbf{L}\,\mathbf{C}$ are placed to lie further on the negative half-plane by calculating an appropriate observer matrix $\mathbf{L}$, [18]. By doing so, the state estimate error $\mathbf{e}(t)$ converges faster to zero than the state vector $\mathbf{x}(t)$ which is necessary for the controller to determine the correct control input $\mathbf{u}(t)$.

4. NUMERICAL SIMULATION

Numerical simulations based on the reduced state space model derived in Sec. 3.2 and the controller design in Sec. 3.3 are conducted to prove the concept of active buckling control by active supports with integrated piezoelectric actuators for supercritical axial loads $P > P_{\text{cr},1}$ illustrated in Figures 1 and 2. The maximum first theoretical critical buckling load of a beam-column with the properties given in Table 1 is achieved for a fixed-fixed beam-column with

$$P_{\text{e}} = \frac{\pi^2 \, EI_{\text{b}}}{(0.5 \, l)^2} = 3472.7 \, \text{N}, \tag{25}$$

representing EULER case IV, [1]. Using the FE-model of the elastically supported beam-column, Fig. 3, derived in Sec. 3.1, the first and second critical buckling loads of the uncontrolled beam-column are calculated by Eq. (6) to

$$\begin{aligned}
P_{\text{cr},1} &= 3122.5 \, \text{N} \approx 0.90 \, P_{\text{e}}, \\
P_{\text{cr},2} &= 6414.8 \, \text{N} \approx 1.85 \, P_{\text{e}}.
\end{aligned} \tag{26}$$

Thus, the beam-column has a slightly lower first critical buckling load than the maximum theoretical critical buckling load P_{e} and the elastic supports with piezoelectric stack actuators are not as stiff as a fixed support.

The active buckling control is demonstrated for the simulation cases given in Table 2. Three different supercritical axial loads P are taken into account: an axial load slightly above the first critical buckling load $P = 3200 \, \text{N} \approx 1.02 \, P_{\text{cr},1}$ (Case A), the maximum bearable axial load above the second critical buckling load $P = 7700 \, \text{N} \approx 1.20 \, P_{\text{cr},2} \approx 2.22 \, P_{\text{e}}$ (Case B) and a medium axial load of $P = 5000 \, \text{N} \approx 1.60 \, P_{\text{cr},1}$ (Case C). Cases A and B present the active stabilization of the supercritically loaded beam-column in the z-direction with disturbance angle $\gamma_{\text{d}} = 90\,^\circ$ according to the coordinates given in Fig. 1b. Case C shows the active buckling control for disturbance angle $\gamma_{\text{d}} = 120\,^\circ$ and a different disturbance force amplitude $\widehat{F}_{\text{d}}$ and position x_{d}, Fig. 1.

Case	A	B	C
P	3200 N	7700 N	5000 N
$\widehat{F}_{\text{d}}$	5 N	5 N	10 N
γ_{d}	90 $^\circ$	90 $^\circ$	120 $^\circ$
x_{d}	0.1 m	0.1 m	0.15 m

Table 2: Numerical simulation cases of the supercritically loaded and stabilized beam-column

The impulse disturbance force $F_{\text{d}}(t)$, Fig. 1b, is approximated by a shifted cosine wave with maximum amplitude $\widehat{F}_{\text{d}}$ and disturbance length $\Delta t_{\text{d}} = 0.001 \, \text{s}$ that starts at time $t = 0.01 \, \text{s}$.

Case A: Figure 5a shows the sensor strains $\varepsilon_z(x_{\mathrm{s},1/2}, t)$ in the z-direction at sensor locations $x_{\mathrm{s},1/2}$, Eq. (16), of the controlled and uncontrolled beam-column. For the uncontrolled system, the beam-column buckles and the initial deflection resulting from the disturbance $F_{\mathrm{d}}(t)$ with $\widehat{F}_{\mathrm{d}} = 5.0\,\mathrm{N}$ and $\gamma_{\mathrm{d}} = 90\,^\circ$, Table 2, quickly grows and becomes inadmissibly high so that the simulation is stopped. For the actively stabilized beam-column, the system does not buckle and after $0.06\,\mathrm{s}$, the surface strain has nearly returned to zero so that the beam-column has almost reached its straight form again. The strain sensor signal is superposed by an oscillation of the second mode shape which is excited by the non-centric disturbance force, $x_{\mathrm{d}} = 0.1\,\mathrm{m}$, and recognized as a counter-phase signal from sensors 1 and 2. Figure 5b shows the control forces $F_{\mathrm{az},1/2}$ for the actively controlled beam-column. The control forces $F_{\mathrm{az,A}}$ and $F_{\mathrm{az,B}}$ with a maximum value of $32\,\mathrm{N}$ are the same and therefore overlap in the figure.

Figure 5: Case A: Axial load $P = 3200\,\mathrm{N} \approx 1.02\,P_{\mathrm{cr},1}$, disturbance force amplitude $\widehat{F}_{\mathrm{d}} = 5.0\,\mathrm{N}$, disturbance angle $\gamma_{\mathrm{d}} = 90\,^\circ$ and disturbance position $x_{\mathrm{d}} = 0.1\,\mathrm{m}$, a) sensor strains $\varepsilon_z(x_{\mathrm{s},1}, t)$ controlled (——) and uncontrolled (– –) and $\varepsilon_z(x_{\mathrm{s},2}, t)$ controlled (——) and uncontrolled (– –), b) controller forces $F_{\mathrm{az,A}}$ (——) and $F_{\mathrm{az,B}}$ (——) for actively controlled beam-column

Case B: The maximum axial load P for which the beam-column is able to be stabilized is $P = 7700\,\text{N} \approx 1.20\,P_{\text{cr},2} \approx 2.22\,P_{\text{e}}$. The stabilization is limited by the maximum controller force of $750\,\text{N}$ for the chosen piezoelectric stack actuators. The disturbance $F_{\text{d}}(t)$ is the same as in Case A, Table 2. Figure 6 again shows the sensor strains $\varepsilon_z(x_{\text{s},1/2},t)$ and control forces $F_{\text{az},A/B}$. Since the axial load is larger than the second critical buckling load $P_{\text{cr},2}$, the beam-column buckles in the second buckling shape and the sensor signal, Fig. 6a, does not show any oscillations and has different signs for sensors 1 and 2. The maximum sensor strains $\varepsilon_z(x_{\text{s},1/2},t)$ are a lot smaller than in Case A. This is due to the fact that the state estimate error converges faster for higher axial loads and the stabilization is faster so that the beam-column is in its straight form again after $0.014\,\text{s}$. However, also the maximum actuator force $F_{\text{az},A} = 743\,\text{N}$ is required for the stabilization. In contrast to Case A, the actuator forces are not equal which can be attributed to the asymmetrical buckling shape.
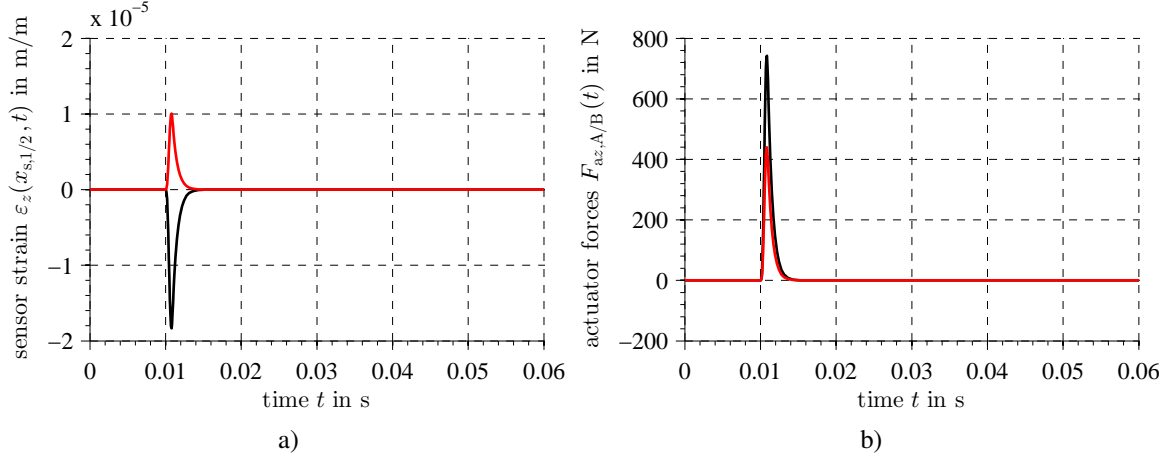

Figure 6: Case B: Axial load $P = 7700\,\text{N} \approx 1.20\,P_{\text{cr},2} = 2.22\,P_{\text{e}}$, disturbance force amplitude $\widehat{F}_{\text{d}} = 5.0\,\text{N}$, disturbance angle $\gamma_{\text{d}} = 90\,^{\circ}$ and disturbance position $x_{\text{d}} = 0.1\,\text{m}$, a) sensor strains $\varepsilon_z(x_{\text{s},1},t)$ (——) and $\varepsilon_z(x_{\text{s},2},t)$ (——), b) controller forces $F_{\text{az},A}$ (——) and $F_{\text{az},B}$ (——) for actively controlled beam-column

Case C: The third simulation case shows both the influence of increasing disturbance force amplitude $\widehat{F}_\mathrm{d} = 10.0\,\mathrm{N}$ and change in angle $\gamma_\mathrm{d} = 120\,^\circ$. Also, the disturbance position is changed to $x_\mathrm{d} = 0.15\,\mathrm{m}$, Table 2. Figure 7a shows the sensor strains $\varepsilon_z(x_{\mathrm{s},1/2}, t)$ and $\varepsilon_y(x_{\mathrm{s},1/2}, t)$ for $\gamma_\mathrm{d} = 120\,^\circ$ that are positive in the y- and negative in the z-direction. The strains $\varepsilon_z(x_{\mathrm{s},1/2}, t)$ are larger than $\varepsilon_y(x_{\mathrm{s},1/2}, t)$ and again show the counter-phase oscillation of the second mode shape. The disturbance in the z-direction is larger than in the y-direction and, consequently, also the required control forces $F_{\mathrm{a}z,1/2}$ are larger than $F_{\mathrm{a}y,1/2}$, Fig. 7b. Because of the higher disturbance force amplitude $\widehat{F}_\mathrm{d}$, the required control force again almost reaches the maximum piezoelectric stack actuator force of $750\,\mathrm{N}$. The numerical simulation shows that the stabilization of the circular beam-column is also possible for different disturbance force angles γ_d in arbitrary direction perpendicular to the x-axis.
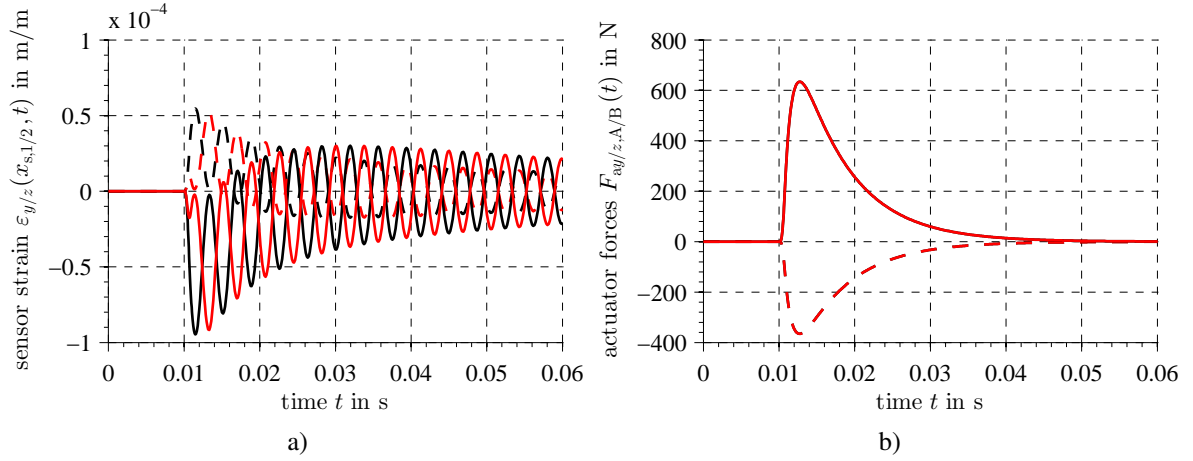

Figure 7: Case C: Axial load $P = 5000\,\mathrm{N} \approx 1.60\,P_{\mathrm{cr},1}$, disturbance force amplitude $\widehat{F}_\mathrm{d} = 10.0\,\mathrm{N}$, disturbance angle $\gamma_\mathrm{d} = 120\,^\circ$ and disturbance position $x_\mathrm{d} = 0.15\,\mathrm{m}$, a) sensor strains $\varepsilon_z(x_{\mathrm{s},1}, t)$ (——), $\varepsilon_z(x_{\mathrm{s},2}, t)$ (——), $\varepsilon_y(x_{\mathrm{s},1}, t)$ (– –), $\varepsilon_y(x_{\mathrm{s},2}, t)$ (– –), b) controller forces $F_{\mathrm{a}z,\mathrm{A}}$ (– –) and $F_{\mathrm{a}z,\mathrm{B}}$ (– –) for actively controlled beam-column

5. CONCLUSIONS

A new method of active buckling control of a beam-column with circular cross-section loaded by a supercritical constant axial load by active supports with integrated piezoelectric stack actuators is presented and investigated numerically. With the active supports, lateral forces in arbitrary directions orthogonal to the beam-column's longitudinal axis can be introduced below the beam-column ends. A reduced modal state space model of a real beam-column test setup is derived and a linear quadratic regulator with state estimator is implemented. The numerical simulation of several case studies shows that active stabilization of the supercritically loaded beam-column with circular cross-section disturbed by a lateral impulse disturbance force is possible up to a 2.47 increase of the first critical buckling load of the uncontrolled beam-column. The numerical simulations show the effectiveness of the active supports with integrated piezoelectric actuators. Further examinations will investigate the implementation of the derived controller on the experimental test setup.

ACKNOWLEDGMENTS

References

[1] Timoshenko, S. P. ; Gere, J. M.: *Theory of Elastic Stability*. McGraw-Hill, New York, 1961.

[2] Meressi, T. ; Paden, B.: Buckling control of a flexible beam using piezoelectric actuators. *Journal of Guidance, Control, and Dynamics*, **16** (5): 977–980, 1993.

[3] Wang, Q. S.: Active buckling control of beams using piezoelectric actuators and strain gauge sensors. *Smart Materials and Structures*, **19**: 1–8, 2010.

[4] Thompson, S. P. ; Loughlan, J.: The active buckling control of some composite column strips using piezoceramic actuators. *Composite Structures*, **32**: 59–67, 1995.

[5] Berlin, A. A. ; Chase, J. G. ; Yim, M. ; Maclean, J. B. ; Olivier, M. ; Jacobsen, S. C.: Mems-based control of structural dynamic instability. *Journal of Intelligent Material Systems and Structures*, **9**: 574– 586, 1998.

[6] Choi, S. ; Lee, J. J. ; Seo, D. C. ; Choi, S. W.: The active buckling control of laminated composite beams with embedded shape memory alloy wires. *Composite Structures*, **47**: 679–686, 1999.

[7] Enss, G. C. ; Platz, R. ; Hanselka, H.: Mathematical modelling of postbuckling in a slender beam column for active stabilisation control with respect to uncertainty. In *Proc. SPIE*, volume 8341, 2012.

[8] Enss, G. C. ; Platz, R. ; Hanselka, H.: Uncertainty in loading and control of an active column critical to buckling. *Shock and Vibration*, **19**: 929–937, 2012.

[9] Enss, G. C. ; Platz, R.: Statistical approach for active buckling control with uncertainty. In *Proc. IMAC XXXII*, number 209, 2014.

[10] Schaeffner, M. ; Enss, G. C. ; Platz, R.: Mathematical modeling and numerical simulation of an actively stabilized beam-column with circular cross-section. In *Proc. SPIE*, volume 9057, 2014.

[11] Klein, B.: *FEM*. Springer Vieweg, Wiesbaden, 2012.

[12] Przemieniecki, J. S.: *Theory of Matrix Structural Analysis*. McGraw-Hill, New York, 1968.

[13] Khot, S. M. ; Yelve, N. P.: Modeling and response analysis of dynamic systems by using ANSYS and MATLAB. *Journal of Vibration and Control*, **0** (0): 1–6, 2010.

[14] Gawronski, W.: *Balanced Control of Flexible Structures*. Springer, London, 1996.

[15] Laub, A. J. ; Heath, M. T. ; Paige, C. C. ; Ward, R. C.: Computation of system balancing transformations and other applications of simultaneous diagonalization algorithms. *IEEE Transactions on Automatic Control*, **32**: 115–122, 1987.

[16] Skogestad, S. ; Postlethwaite, I.: *Multivariable Feedback Control: Analysis and Design*. John Wiley & Sons, New York, 2005.

[17] Adamy, J.: *Systemdynamik und Regelungstechnik II*. Shaker, Aachen, 2007.

[18] Lunze, J.: *Regelungstechnik 2 Mehrgrößensysteme, Digitale Regelung*. Springer-Verlag Berlin Heidelberg, 2008.